Turkish Journal of Engineering & Environmental Sciences

http://journals.tubitak.gov.tr/engineering/

Research Article

Turkish J Eng Env Sci
(2013) 37: 162 – 177

doi:10.3906/muh-1205-14

Finite element analysis of frictional contact of elastic solids with thin and moderately thick coatings

Bahattin KANBER[1,*] **Necdet DEMİRHAN**[2]

[1]Mechanical Engineering Department, Gaziantep University, Gaziantep, Turkey

[2]Department of Machine and Metal Technologies, Gaziantep Vocational School, Gaziantep University, Gaziantep, Turkey

Received: 28.05.2012 • **Accepted:** 26.03.2013 • **Published Online:** 04.07.2013 • **Printed:** 29.07.2013

Abstract: The frictional contact of elastic solids with thin and moderately thick coatings is analysed by using the finite element method. It is assumed that 2 elastic, homogeneous substrates with elastic coatings are perfectly bonded and contact with each other under normal and horizontal forces. The coating and elastic substrate are modelled with 2D and 3D finite elements. After verifying the finite element solutions by analytical solutions, various geometric configurations are analysed such as ball and socket joint, ball on a flat plate, a roller on a guide, and spur gear. Different material combinations and coating thicknesses are considered in the coating–substrate system. Their effects on the total displacement and contact stress distributions along the contact line of coated members are presented.

Key words: Frictional contact problems, elastic substrate, thin coating, moderately thick coating, finite element method, ball and socket joint, ball on a plate, roller on a guide, spur gear, contact stress, contact displacement

1. Introduction

It is known that many failures in structural components are caused by contact stresses. Therefore, the surfaces in contact are the main concern of many researchers (Johnson, 1985; Wriggers, 2002). Coating is one of the methods of improving the surface mechanical properties of the members and is widely used in industry (Lindsay, 1998). Elastic coating stresses were analytically studied by Gupta et al. (1973), O'Sullivan and King (1988), and Leroy and Villechaise (1990). Thin-coating contact mechanics theory was proposed by Reedy (2006) by assuming that the elastic modulus of coating is much less than the elastic modulus of substrates. When the elastic modulus of coating and substrate are comparable, the theory must be modified using some constants (Hsueh, 2004). In addition to this theory, some experimental techniques are developed and used to determine the mechanical properties of thin coatings in coating and substrate systems (Shieu and Shiao, 1997). Numerical techniques, such as the finite element method (FEM) and boundary element method (BEM), are also widely used in the analysis of contact mechanic problems with thin coating (Komvopoulos, 1988; Hong and Saka, 1991; Djabella and Arnell, 1993; Sun et al., 1995; Njiwa et al., 1998; Diao and Kandori, 2006). The thin-coating technique is generally used in structural components such as gears, bearings, machine tools, and artificial hip joints to improve their surface mechanical properties (Sen et al., 1989; Liu et al., 2003; Yonekura et al., 2005; Bruno et al., 2006; Martins et al., 2006). Therefore, in this paper, thin-coated joints such as ball and socket, ball on a flat plate, roller on a guide, and spur gear are analysed by FEM. The total displacements and contact

*Correspondence: kanber@gantep.edu.tr

stresses are investigated along the contact line of the coated members for different material combinations and coating thicknesses with friction.

2. Theory of thin-coating contact mechanics

The theory of thin-coating contact mechanics is well described using a spherical indenter, a thin coating, and a flat substrate system (Reedy, 2006). The indenter and substrate are assumed to be rigid and the coating is assumed to be linearly elastic and perfectly bonded on the substrate (Figure 1). The coating has a thickness of h and its elastic properties are described by Young's modulus, E_c, and Poisson's ratio, ν_c. The incompressible coatings are not considered in this theory. The spherical rigid indenter has a radius of R. Since it is pushed into the coating, the indenter approach, w, is taken as positive. The interaction of coating and indenter is assumed to be frictionless. Under these conditions, the contact radius, a, can be determined by

$$a = \sqrt{2Rw} \tag{1}$$

with the assumptions that h/R and a/R are much less than 1, while a/h is much greater than 1. The compressive normal strain, ϵ_z, is dependent on the geometry of the indenter and can be assumed as uniform through the coating thickness. It is given by Reddy (2006) as

$$\epsilon_z(r) = -\frac{a^2}{2Rh}[1 - (\frac{r}{a})^2], \tag{2}$$

where h is the coating thickness and r is the radial distance along the surface of the coating with the origin at the initial point of contact. The compressive stress, σ_z, is as follows:

$$\sigma_z = E_e \epsilon_z \tag{3}$$

where $E_e = \frac{(1-\upsilon_c)E_c}{(1+\upsilon_c)(1-2\upsilon_c)}$ and E_c and υ_c are material constants of coating.

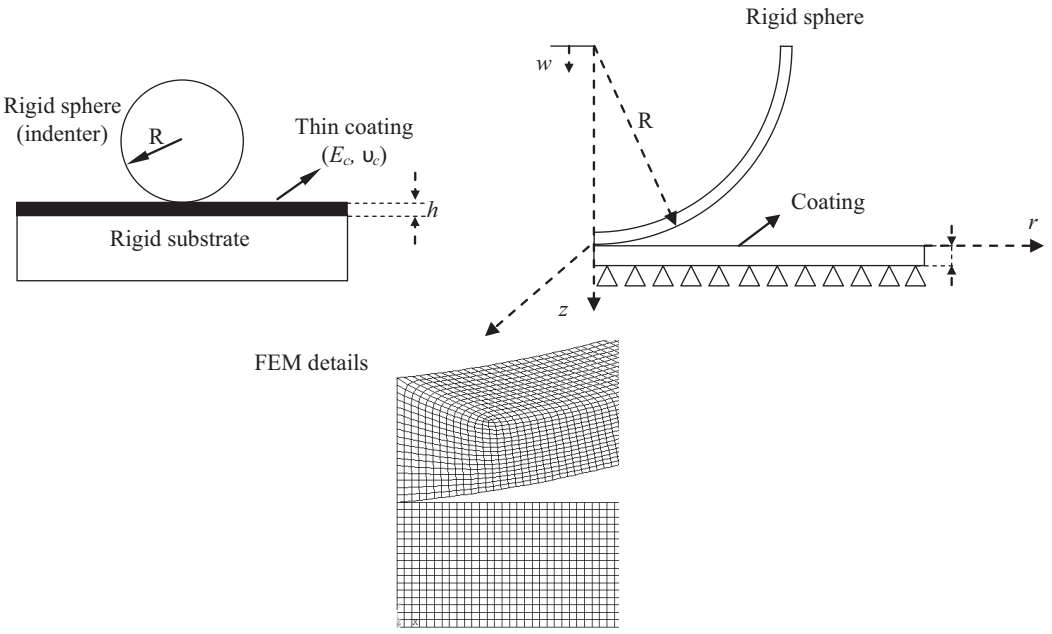

Figure 1. Thin-coating contact model and its FEM model using axi-symmetric elements.

Eqs. (1), (2), and (3) are valid if the materials of indenter and substrate are harder than the coating material. If the substrate material is comparable with the coating material, these equations must be modified (Hsueh, 2004).

3. Finite element analysis

The model, which is solved using the thin-coating contact mechanics theory, is also solved using the commercial finite element package ANSYS. After verifications, all remaining models are only solved in ANSYS. The PLANE82 and SOLID185 elements from the ANSYS element library are used in finite element models. All models are analysed using the Newton–Raphson solution algorithm under static loading conditions. The contact regions are modelled using the TARGE169 and CONTA172 elements for 2D solutions and the TARGE170 and CONTA174 elements for 3D solutions. In order to obtain a converged solution, the elements are continuously refined.

In all models, it is assumed that the coating and substrate are perfectly bonded to each other. Various materials are considered for substrates and coatings. Plots are developed for constant Poisson's ratio ($\upsilon_{s1} = \upsilon_{c1} = \upsilon_{s1} = \upsilon_{c2} = 0.3$), different Young's modulus ratios, $E_u = \frac{E_{c1}}{E_{s1}}$, $E_l = \frac{E_{c2}}{E_{s2}}$, and different coating thickness ratios, $h_r = \frac{h_2}{h_1}$.

4. Solutions and discussion

The solutions have been obtained by means of a PC. The hardware configuration consists of an Intel Pentium IV 2.4 GHz CPU, 2 Gb RAM.

4.1. Comparison of thin-coating contact mechanics theory and FEM

A thin-coating contact model (Hsueh, 2004; Reedy, 2006) is used to compare the theory with the FEM solution (Figure 1). The contact radius, a, can be directly determined by Eq. (1), if the material of substrate and indenter is much harder than the coating material. The FEM model is also shown in Figure 1. Because of axi-symmetry, only the cross section is modelled. The indenter and substrate are assumed to be rigid. To simulate a rigid substrate, a constraint is applied at the bottom of the coating in the z-direction. For simplicity, the indenter radius, R, is taken as 10 mm. Material constants of coating are used as $E_c = 69\,GPa$ and $\upsilon_c = 0.4$. The coefficient of friction, μ, in the contact area is assumed to be zero. The results are plotted as the ratios of coating thickness (h) to indenter radius (R) and prescribed displacement (w) to contact radius (a). The thin-coating theory results deviate from FEM results when the h/R ratio becomes greater than 0.05, as shown in Figure 2. This may be regarded as normal because the thin-coating theory must be modified when the thickness of the coating is comparable with the radius of the indenter.

4.2. Ball and socket joint

Because of friction, ball and socket joints are modelled using 3D finite elements, as shown in Figure 3. Since the upper half of the ball has no contact under load, its lower half is used in the model. In order to overcome the convergence problems, the vertical force is applied as prescribed displacement, w, at the symmetry surface of the ball. The socket is fixed at the bottom surface. The ball and socket are considered as substrates (s_1 and s_2) and their coatings (c_1 and c_2) are assumed to be perfectly bonded. The coatings have thicknesses of h_1 and h_2.

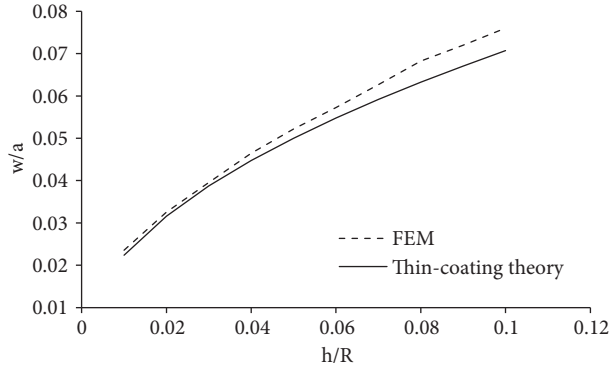

Figure 2. Comparison of thin-coating theory and FEM ($\mu = 0$).

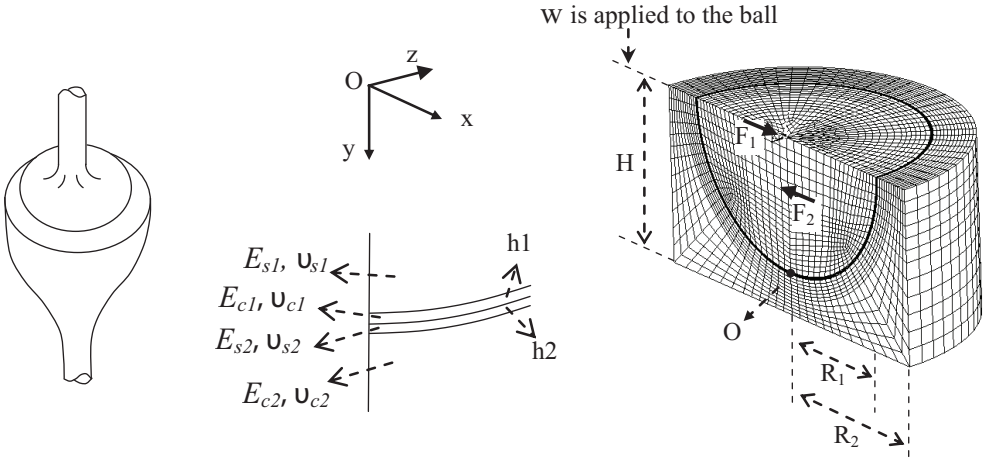

Figure 3. Ball and socket joint with thin coating and its FEM model using 3D elements ($R_1 = 50$ mm, $R_2 = 1.3 \times R_1$, $H = 1.3 \times R_1$, $\mu = 0$ and 0.3, half-view represented).

A parametric model is developed with the dimensions and material constants shown in Table 1. The model is initially solved without friction to represent its effect. Then it is also solved with friction and under the action of horizontal loads. The moment that is created by horizontal loads causes rotation and creates convergence problems. To eliminate this effect, 2 opposite horizontal forces, F_1 and F_2, are applied to the ball for obtaining frictional load at the contact surface as follows:

Table 1. Dimensions, material constants, and loadings for ball and socket joint.

R_1 (mm)	50
R_2 (mm)	$1.3 \times R_1$
H (mm)	$1.3 \times R_1$
h_1, h_2 ($\times R_1$, mm)	$\frac{1}{25}$, $\frac{1}{50}$, $\frac{1}{100}$
E_{s1}, E_{s2} (GPa)	200
E_{c1}, E_{c2} (GPa)	400, 200, 100
υ_{s1}, υ_{c1}, υ_{s2}, υ_{c2}	0.3
w (mm)	$R_1/5000$

F_1 is applied at $x = 0$ and $y = R_1$

F_2 is applied at $x = 0$ and $y = R_1/2$

The values of these horizontal forces are obtained from the horizontal force equilibrium Fx = 0.5 $\times\mu\times$ Fy = F_2 – F_1 and moment equilibrium about the origin of coordinates. To reduce the convergence time of finite element solutions, the applied net horizontal load is taken as half of the multiplication of coefficient of friction, μ, and Fy. Fy is the resultant normal force that is created at the contact line under the action of w. The values of Fy depend on the materials and coating thicknesses and change for each case. They are listed in Tables 2 and 3 for the ball and socket joint.

Table 2. Values of Fy for ball and socket joint for w = R_1/5000 and various Eu and El ratios.

Eu	El	Fy (N)
2	2	232,360
2	1	229,900
2	0.5	227,180
1	2	230,700
1	1	228,640
1	0.5	225,950

Table 3. Values of Fy for ball and socket joint for w = R_1/5000 and various hr ratios.

Hr	Fy (N)
100/25	239,370
100/50	234,850
100/100	232,360
50/100	234,010
25/100	237,010

The total displacement at the point O on the contact line in the x–y plane does not change significantly as the friction changes without horizontal load, as shown in Figure 4. However, it decreases at the edges of the contact line due to friction. The deformation of a part can be defined as the difference in nodal displacements of border nodes. Therefore, the deformation of upper and lower part can be written respectively as $\delta^i_{upper} = U^i_{sum} - U^i_{top}$ and $\delta^i_{lower} = U^i_{base} - U^i_{sum}$. U^i_{sum} is the nodal displacements of the contact line and can be found by finite element solutions. U^i_{top} and U^i_{base} are the nodal total displacements of the top line of the upper part and the base line of the lower part, respectively, and i shows a node number. For the ball and socket joint, $U^i_{top} = w$, $U^i_{base} = 0$. The relationship between prescribed displacement (w) and nodal displacements of the contact line can be obtained as $w = U^i_{base} - \delta^i_{upper} - \delta^i_{lower}$. For this case, the upper part is the ball and its deformation distribution is shown in Figure 4. It is observed that socket deformation is nearly equal to 25% of w. In the case of friction and horizontal load, the total displacement decreases in the direction of the applied horizontal load, and increases in the opposite direction. Similar effects of friction are observed for the normal stress distributions, as shown in Figure 5. Tangential stress significantly decreases around the point O with friction, and when the horizontal load is applied, it shifts in the horizontal load direction (Figure 6). Horizontal loads cause asymmetric stress distributions. Similar effects are reported by Guler and Erdogan (2006) and Ke and Wang (2007) in frictional contact analysis of functionally graded coated members.

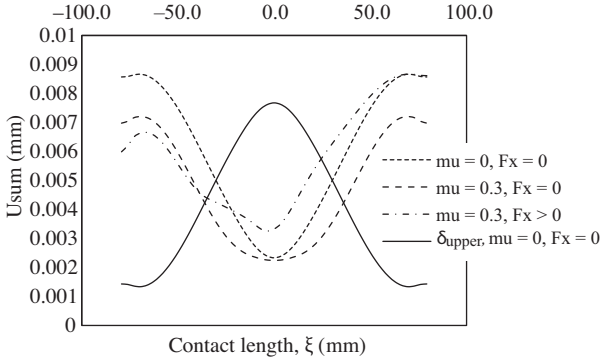

Figure 4. Total displacement distributions along contact line of ball and socket in the x–y plane for different friction and horizontal load cases ($R_1 = 50$ mm, $R_2 = 1.3 \times R_1$, $H = 1.3 \times R_1$, $E_u = E_l = 1$, $h_1 = R_2/100$, $h_2 = R_2/100, h_r = 100/100$, $\mu = 0$ and 0.3) and deformation distribution of the ball for the frictionless case.

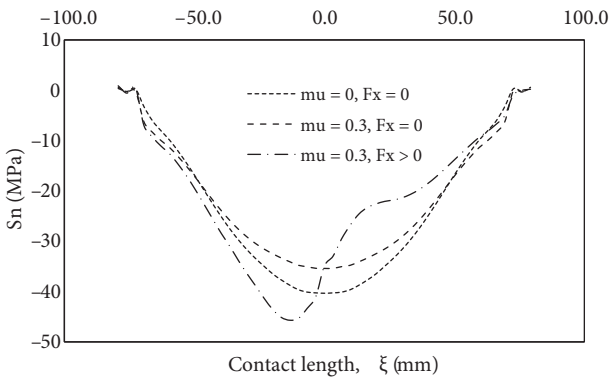

Figure 5. Normal stress distributions along the contact line of ball and socket in the x–y plane for different friction and horizontal load cases ($R_1 = 50$ mm, $R_2 = 1.3 \times R_1$, $H = 1.3 \times R_1$, $E_u = E_l = 1$, $h_1 = R_2/100$, $h_2 = R_2/100, h_r = 100/100$, $\mu = 0$ and 0.3).

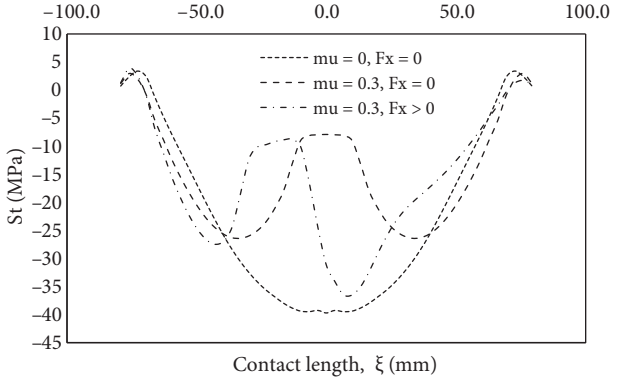

Figure 6. Tangential stress distributions along the contact line of ball and socket in the x–y plane for different friction and horizontal load cases ($R_1 = 50$ mm, $R_2 = 1.3 \times R_1$, $H = 1.3 \times R_1$, $E_u = E_l = 1$, $h_1 = R_2/100$, $h_2 = R_2/100, h_r = 100/100$, $\mu = 0$ and 0.3).

The Young's modulus ratios, E_u and E_l, do not have a significant effect on the total displacement or normal stress distributions, as shown in Figures 7 and 8. The tangential stress distributions are grouped according to the elastic modulus ratio of the ball. For the harder coating group, the tangential stress decreases around the point O and increases immediately in the vicinity of this region, as shown in Figure 9. The coating thickness ratios, h_r, have similar effects, as shown in Figures 10–12.

4.3. A ball on a flat plate

A ball on a flat plate is an example of nonconforming contact. Although the geometry is suitable for axisymmetric modelling, the frictional loads require a 3D model for this application. Therefore, 3D FEs are used in the model, as shown in Figure 13. The plate is fixed at the bottom face. The vertical and horizontal loads are applied as in the previous case. The parameters and their values are given in Tables 4–6.

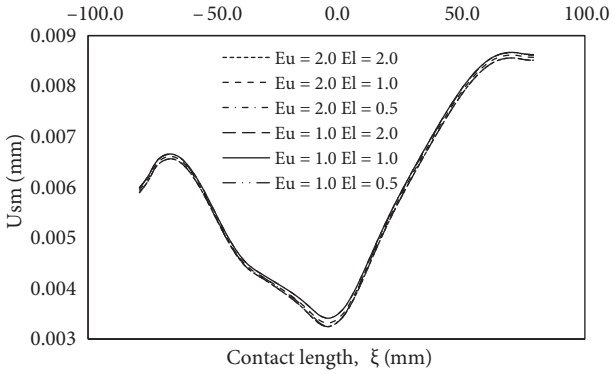

Figure 7. Total displacement distributions along the contact line of ball and socket in the x–y plane for various Young's modulus ratios ($R_1 = 50$ mm, $R_2 = 1.3 \times R_1$, $H = 1.3 \times R_1$, $h_1 = R_2/100$, $h_2 = R_2/100$, $h_r = 100/100$, $\mu = 0.3$).

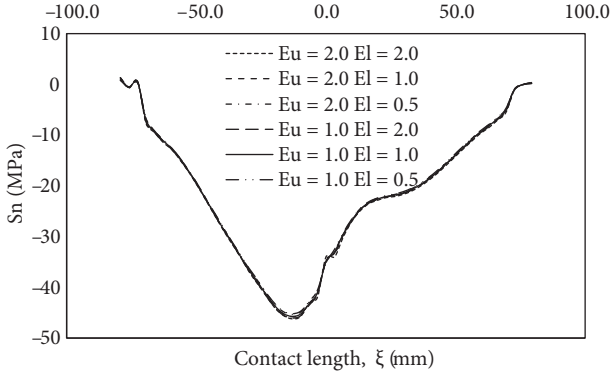

Figure 8. Normal stress distributions along the contact line of ball and socket in the x–y plane for various Young's modulus ratios ($R_1 = 50$ mm, $R_2 = 1.3 \times R_1$, $H = 1.3 \times R_1$, $h_1 = R_2/100$, $h_2 = R_2/100, h_r = 100/100$, $\mu = 0.3$).

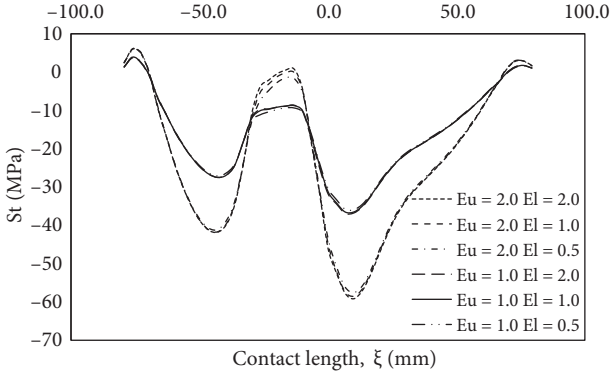

Figure 9. Tangential stress distributions along the contact line of ball and socket in the x–y plane for various Young's modulus ratios ($R_1 = 50$ mm, $R_2 = 1.3 \times R_1$, $H = 1.3 \times R_1$, $h_1 = R_2/100$, $h_2 = R_2/100, h_r = 100/100$, $\mu = 0.3$).

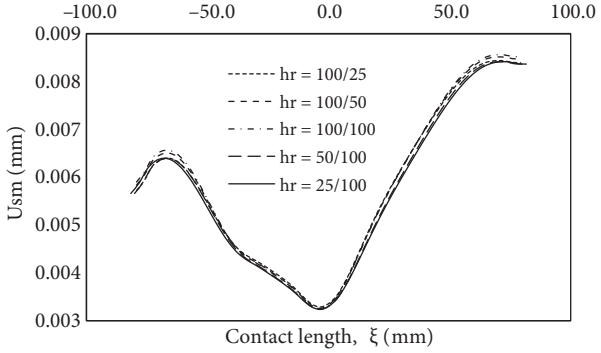

Figure 10. Total displacement distributions along the contact line of ball and socket in the x–y plane for various coating thickness ratios ($R_1 = 50$ mm, $R_28 = 1.3 \times R_1$, $H = 1.3 \times R_1$, $E_u = E_l = 2$, $\mu = 0.3$).

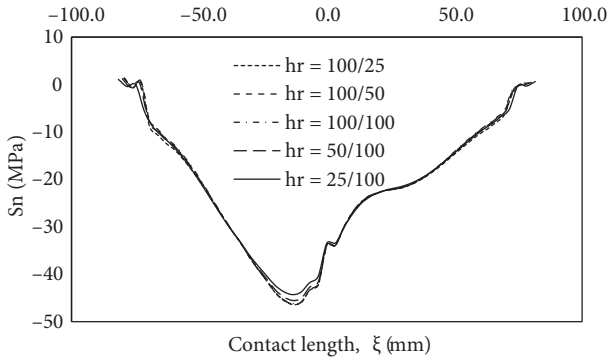

Figure 11. Normal stress distributions along the contact line of ball and socket in the x–y plane for various coating thickness ratios ($R_1 = 50$ mm, $R_2 = 1.3 \times R_1$, $H = 1.3 \times R_1$, $E_u = E_l = 2$, $\mu = 0.3$).

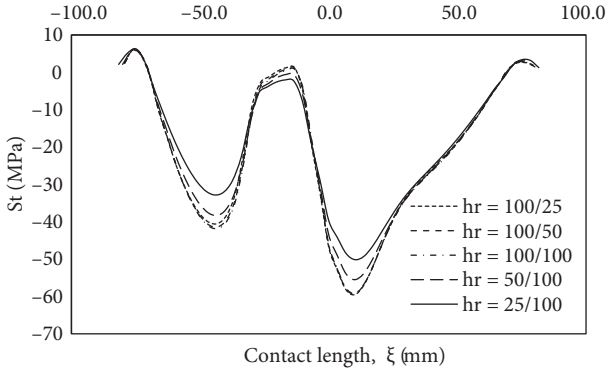

Figure 12. Tangential stress distributions along the contact line of ball and socket in the x–y plane for various coating thickness ratios ($R_1 = 50$ mm, $R_2 = 1.3 \times R_1$, $H = 1.3 \times R_1$, $E_u = E_l = 2$, $\mu = 0.3$).

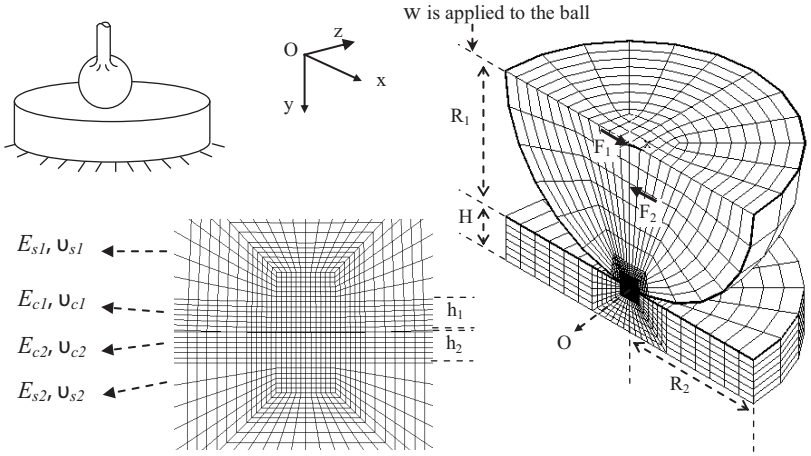

Figure 13. Ball on a plate with thin coating and its FEM model using 3D elements ($R_1 = 50$ mm, $R_2 = R_1$, $H = 0.3 \times R_1$, $\mu = 0.3$, half-view represented).

Table 4. Dimensions, material constants, and loadings for ball on a plate model.

R_1 (mm)	50
R_2 (mm)	R_1
H (mm)	$0.3 \times R_1$
h_1, h_2 ($\times R_1$, mm)	$\frac{1}{25}$, $\frac{1}{50}$, $\frac{1}{100}$
E_{s1}, E_{s2} (GPa)	200
E_{c1}, E_{c2} (GPa)	400, 200, 100
$\upsilon_{s1}, \upsilon_{c1}, \upsilon_{s2}, \upsilon_{c2}$	0.3
w (mm)	$R_1/5000$

Table 5. Values of Fy for ball on a plate model for w = $R_1/5000$ and various Eu and El ratios.

Eu	El	Fy (N)
2	2	1308.5
2	1	1174.4
2	0.5	1007
1	2	1173.4
1	1	1072.7
1	0.5	930.3

Table 6. Values of Fy for ball on a plate model for w = $R_1/5000$ and various hr ratios.

Hr	Fy (N)
100/25	1486.7
100/50	1407.2
100/100	1308.5
50/100	1407.9
25/100	1499.2

The largest deformations of contacting parts are obtained inside the contact region and their values decrease outside of the region. While the deformations approach zero, the nodal displacements approach the prescribed displacements, as shown in Figure 14. Therefore, the nodal displacements approach similar values near the contact corner in the ball and socket joint and outside the contact region in the ball on a plate case. In addition, as the ratio of $\frac{E_u}{E_l}$ increases, the total displacement distributions also increase. When E_l is constant, normal stresses increase as E_u increases. Increasing E_l also causes increases in the normal stresses (Figure 15). However, E_l and E_u have a reverse effect on tangential stress distributions, as shown in Figure 16.

Although increasing the coating thickness ratio, h_r, decreases the total displacement, it causes increasing normal and tangential stress distributions, as shown in Figures 17–19.

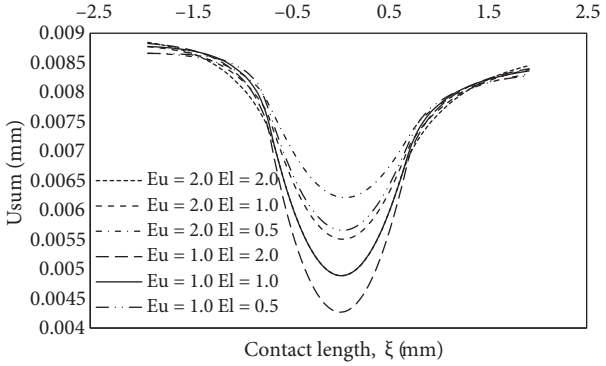

Figure 14. Total displacement distributions along the contact line of ball and plate in the x–y plane for various Young's modulus ratios ($R_1 = 50$ mm, $R_2 = R_1$, $H = 0.3 \times R_1$, $h_1 = R_2/100$, $h_2 = R_2/100, h_r = 100/100$, $\mu = 0.3$).

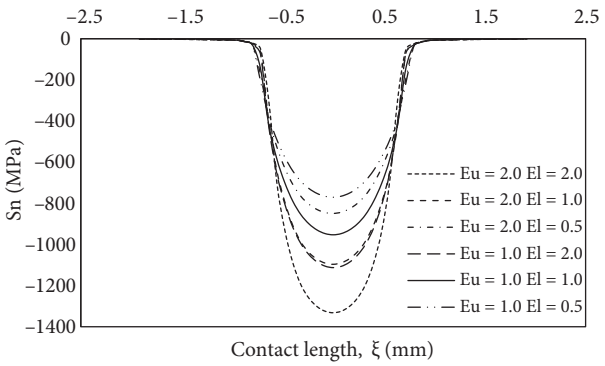

Figure 15. Normal stress distributions along the contact line of ball and plate in the x–y plane for various Young's modulus ratios ($R_1 = 50$ mm, $R_2 = R_1$, $H = 0.3 \times R_1$, $h_1 = R_2/100$, $h_2 = R_2/100, h_r = 100/100$, $\mu = 0.3$).

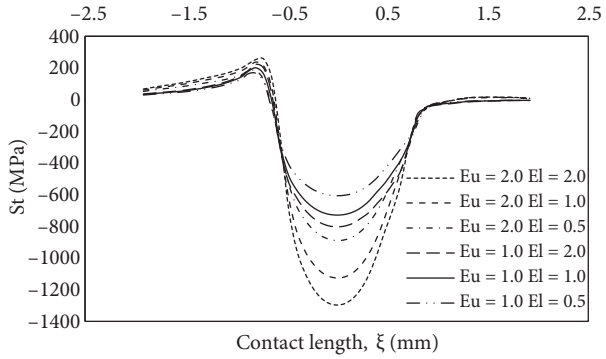

Figure 16. Tangential stress distributions along the contact line of ball and plate in the x–y plane for various Young's modulus ratios ($R_1 = 50$ mm, $R_2 = R_1$, $H = 0.3 \times R_1$, $h_1 = R_2/100$, $h_2 = R_2/100, h_r = 100/100$, $\mu = 0.3$).

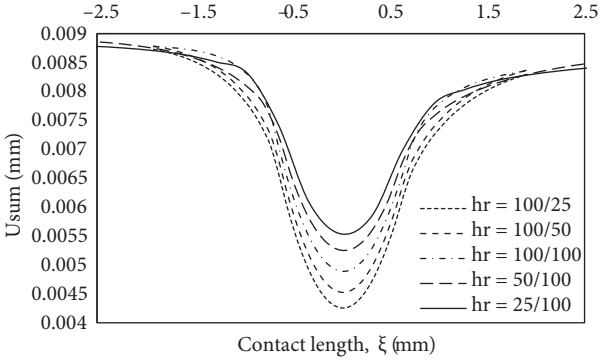

Figure 17. Total displacement distributions along the contact line of ball and plate in the x–y plane for various coating thickness ratios ($R_1 = 50$ mm, $R_2 = R_1$, $H = 0.3 \times R_1, E_u = E_l = 2$, $\mu = 0.3$).

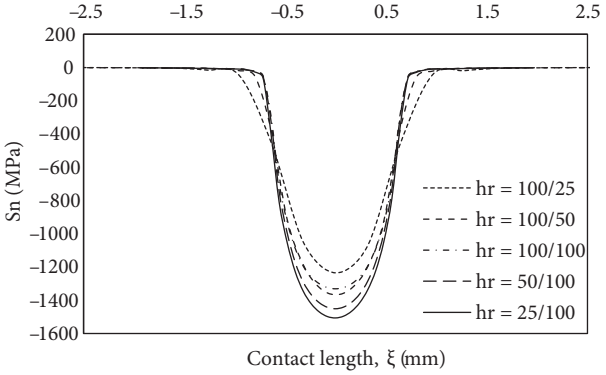

Figure 18. Normal stress distributions along the contact line of ball and plate in the x–y plane for various coating thickness ratios ($R_1 = 50$ mm, $R_2 = R_1$, $H = 0.3 \times R_1$, $E_u = E_l = 2$, $\mu = 0.3$).

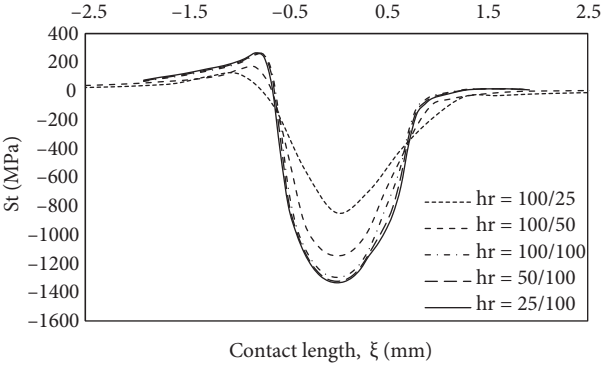

Figure 19. Tangential stress distributions along the contact line of ball and plate in the x–y plane for various coating thickness ratios ($R_1 = 50$ mm, $R_2 = R_1$, $H = 0.3 \times R_1$, $E_u = E_l = 2$, $\mu = 0.3$).

4.4. A roller on a guide

The roller and guide are modelled with 2D elements with plane strain options. It is also a nonconforming contact. The finite element model is shown in Figure 20 and its parameters are given in Tables 7–9. The loads and constraints are applied as in the previous 2 cases. They are applied on lines instead of on surfaces.

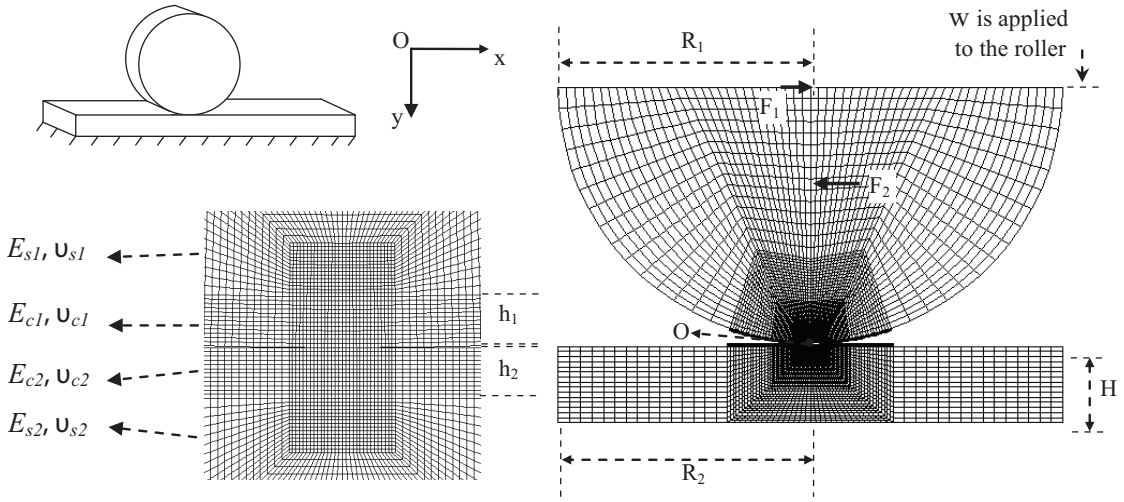

Figure 20. A roller on a guide with thin coating and its FEM model using 2D elements ($R_1 = 50$ mm, $R_2 = R_1$, $H = 0.3 \times R_1$, $\mu = 0.3$).

Table 7. Dimensions, material constants, and loadings for roller on a guide model.

R_1 (mm)	50
R_2 (mm)	R_1
H (mm)	$0.3 \times R_1$
h_1, h_2 ($\times R_1$, mm)	$\frac{1}{25}$, $\frac{1}{50}$, $\frac{1}{100}$
E_{s1}, E_{s2} (GPa)	200
E_{c1}, E_{c2} (GPa)	400, 200, 100
υ_{s1}, $\upsilon_{c1}, \upsilon_{s2}$, υ_{c2}	0.3
w (mm)	$R_1/5000$

Table 8. Values of Fy for roller on a guide model for w = $R_1/5000$ and various Eu and El ratios.

Eu	El	Fy (N)
2	2	385,560
2	1	367,880
2	0.5	342,390
1	2	367,430
1	1	352,300
1	0.5	329,670

Table 9. Values of Fy for roller on a guide model for w = $R_1/5000$ and various hr ratios.

Hr	Fy (N)
100/25	390,460
100/50	399,080
100/100	385,560
50/100	397,370
25/100	410,440

The total displacements and normal and tangential stresses have distributions similar to the displacements and stresses of the ball on a flat plate case, as shown in Figures 21–26. In this case, the coating thickness ratio is less effective than in the ball on a flat plate case, as shown in Figures 24–26.

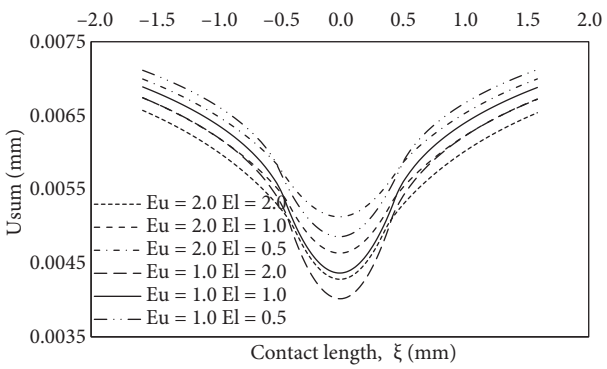

Figure 21. Total displacement distributions along the contact line of roller and guide for various Young's modulus ratios ($R_1 = 50$ mm, $R_2 = R_1$, $H = 0.3 \times R_1$, $h_1 = R_2/100$, $h_2 = R_2/100, h_r = 100/100$, $\mu = 0.3$).

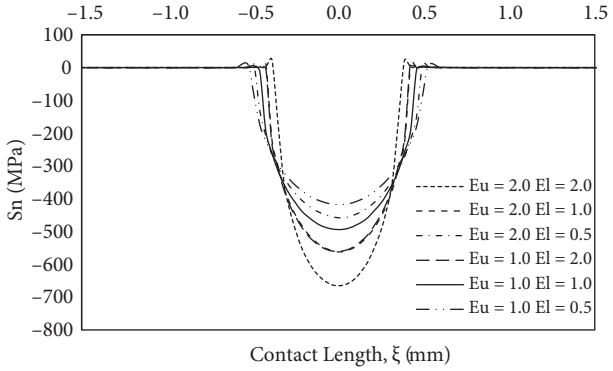

Figure 22. Normal stress distributions along the contact line of roller and guide for various Young's modulus ratios ($R_1 = 50$ mm, $R_2 = R_1$, $H = 0.3 \times R_1$, $h_1 = R_2/100$, $h_2 = R_2/100, h_r = 100/100$, $\mu = 0.3$).

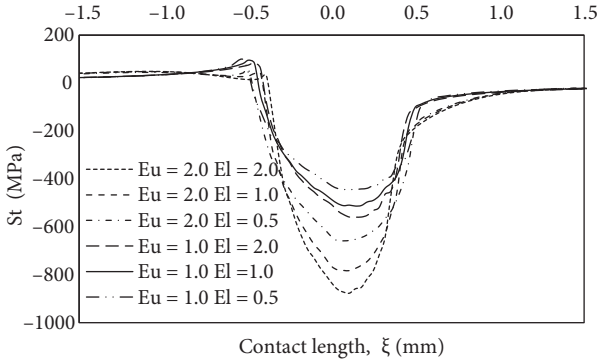

Figure 23. Tangential stress distributions along the contact line of roller and guide for various Young's modulus ratios ($R_1 = 50$ mm, $R_2 = R_1$, $H = 0.3 \times R_1$, $h_1 = R_2/100$, $h_2 = R_2/100, h_r = 100/100$, $\mu = 0.3$).

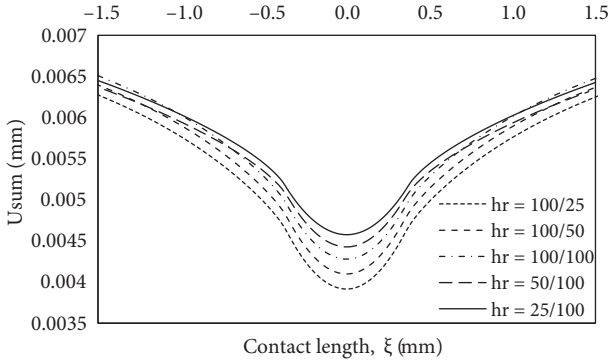

Figure 24. Total displacement distributions along the contact line of roller and guide for various coating thickness ratios ($R_1 = 50$ mm, $R_2 = R_1$, $H = 0.3 \times R_1$, $E_u = E_l = 2$, $\mu = 0.3$).

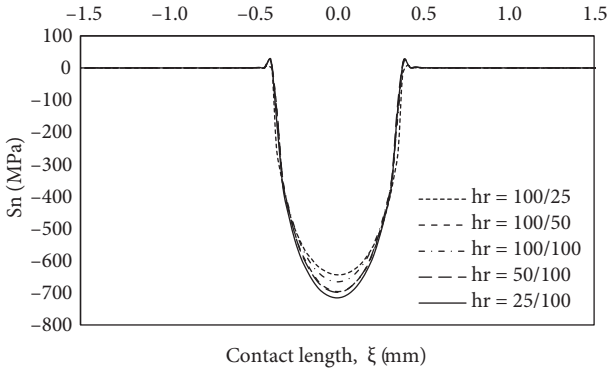

Figure 25. Normal stress distributions along the contact line of roller and guide for various coating thickness ratios ($R_1 = 50$ mm, $R_2 = R_1$, $H = 0.3 \times R_1$, $E_u = E_l = 2$, $\mu = 0.3$).

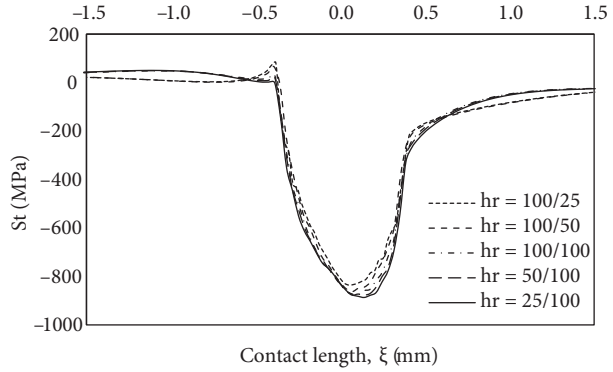

Figure 26. Tangential stress distributions along the contact line of roller and guide for various coating thickness ratios ($R_1 = 50$ mm, $R_2 = R_1$, $H = 0.3 \times R_1$, $E_u = E_l = 2$, $\mu = 0.3$).

4.5. Spur gear

Spur gears are widely used in industry and coated gears are studied by some researchers (Bruno et al., 2006; Martins et al., 2006). The contact displacements and stress characteristics of spur gears can be changed by coating. A FE model is obtained using plane stress elements, as shown in Figure 27. A tooth interaction model is used for simulating whole gear interactions (Kanber, 2006). One tooth is assumed to be the driver and the other tooth is assumed to be driven. The torque is applied at the rigid shaft of the driver tooth. Symmetry roller supports are considered along the left and right sides of the driven tooth. The parameters and their values are given in Table 10.

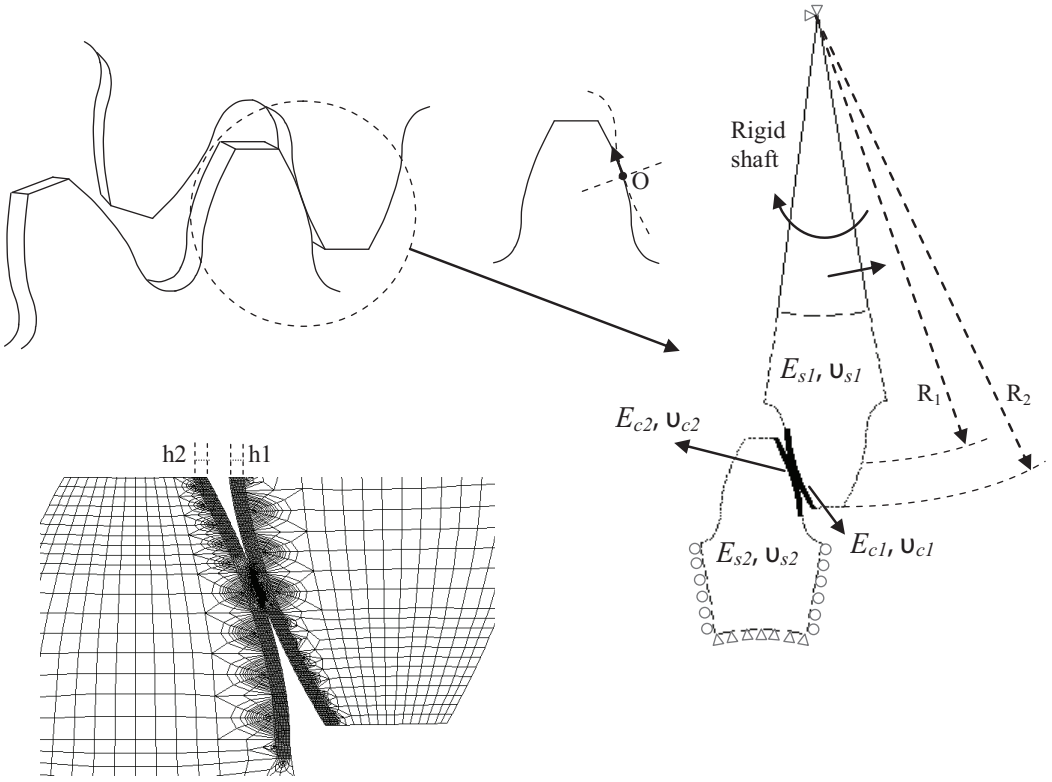

Figure 27. Spur gear and its FEM model using 2D elements ($\mu = 0.3$, plain stress).

Table 10. Dimensions, material constants, and loadings for spur gear model.

	Spur gear
Number of teeth	18
Module	25
Pressure angle (°)	20
Pitch radius, R_1 (mm)	225
Addendum circle radius, R_2 (mm)	250
h_1, h_2 ($\times R_2$, mm)	$\frac{1}{125}, \frac{1}{250}, \frac{1}{500}$
E_{s1}, E_{s2} (GPa)	200
E_{c1}, E_{c2} (GPa)	400, 200, 100
υ_{s1}, $\upsilon_{c1}, \upsilon_{s2}$, υ_{c2}	0.3
T (Nm)	211.5

All displacements and stresses used in plots are taken from the contact line of the driven gear. The Young's modulus ratio of the driver tooth, E_u, is the main affecting parameter in the displacements and contact stresses. The displacements along the contact line of the driven gear decrease when E_u increases, as shown in Figure 28. In ball and roller joints, the displacement distributions show a convex curve. However, the displacement distributions show a concave curve for the driven gear, as shown in Figure 28. As in ball and roller joints, the displacements show a convex curve for the driver gear, as shown in Figure 29. The normal and tangential stresses increase as E_u increases (Figures 30 and 31). They have negative values when the driver and driven gears are in contact. However, when contact is lost between them, the stresses have positive values. Increasing E_l also increases the normal stress. The distribution characteristic of the tangential stress is nearly the same as that of the normal stress.

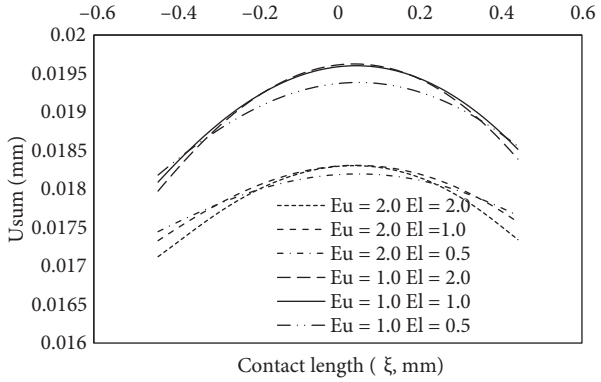

Figure 28. Total displacement distributions along the contact line of the driven gear for various Young's modulus ratios ($R_1 = 225$ mm, $R_2 = 250$ mm, $h_1 = R_2/500$, $h_2 = R_2/500$, $h_r = 500/500$, $\mu = 0.3$).

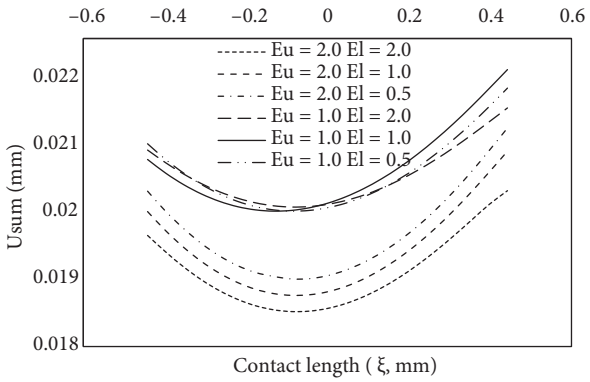

Figure 29. Total displacement distributions along the contact line of the driver gear for various Young's modulus ratios ($R_1 = 225$ mm, $R_2 = 250$ mm, $h_1 = R_2/500$, $h_2 = R_2/500$, $h_r = 500/500$, $\mu = 0.3$).

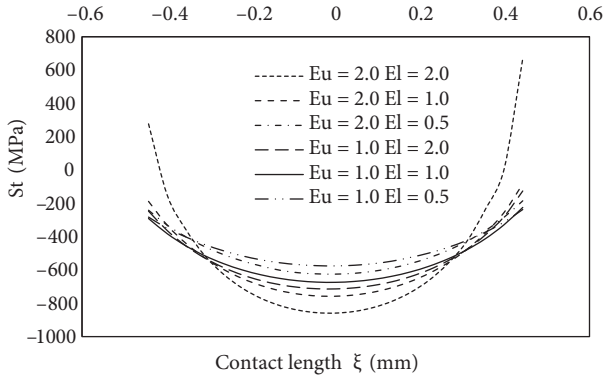

Figure 30. Normal stress distributions along the contact line of the driven gear for various Young's modulus ratios ($R_1 = 225$ mm, $R_2 = 250$ mm, $h_1 = R_2/500$, $h_2 = R_2/500, h_r = 500/500$, $\mu = 0.3$).

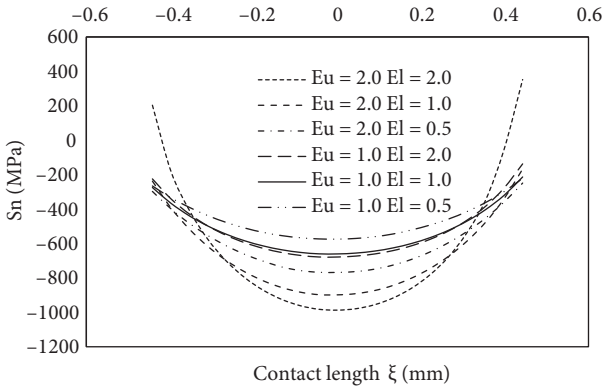

Figure 31. Tangential stress distributions along the contact line of the driven gear for various Young's modulus ratios ($R_1 = 225$ mm, $R_2 = 250$ mm, $h_1 = R_2/500$, $h_2 = R_2/500$, $h_r = 500/500$, $\mu = 0.3$).

The displacements along the contact line of the gear tooth can be significantly reduced by increasing the coating thickness ratio, h_r. When it is less than 1, the displacement distributions are nearly the same, as shown in Figures 32 and 33. The normal stresses increase as h_r increases (Figure 34). However, the tangential stress does not change significantly with h_r, as shown in Figure 35.

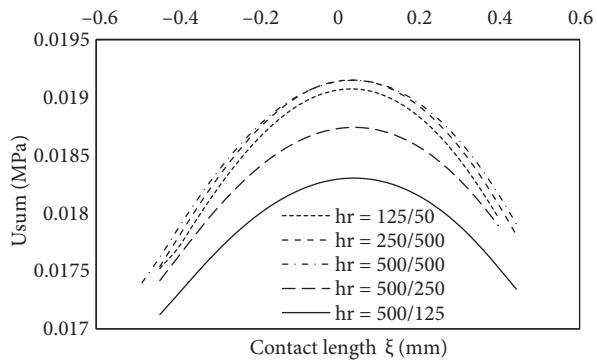

Figure 32. Total displacement distributions along the contact line of the driven gear for various coating thickness ratios ($R_1 = 225$ mm, $R_2 = 250$ mm, $E_u = E_l = 2$, $\mu = 0.3$).

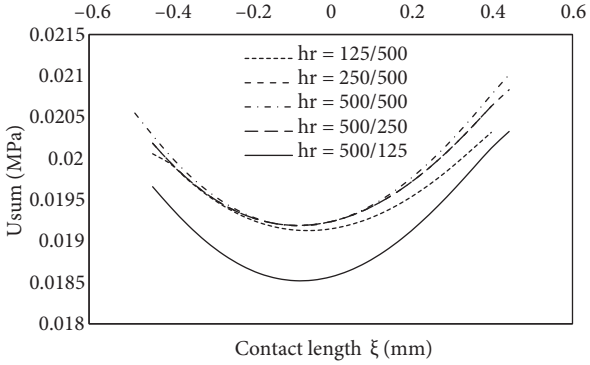

Figure 33. Total displacement distributions along the contact line of the driver gear for various coating thickness ratios ($R_1 = 225$ mm, $R_2 = 250$ mm, $E_u = E_l = 2$, $\mu = 0.3$).

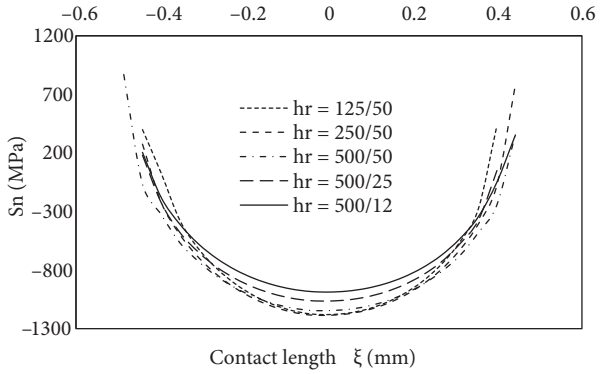

Figure 34. Normal stress distributions along the contact line of the driven gear for various coating thickness ratios ($R_1 = 225$ mm, $R_2 = 250$ mm, $E_u = E_l = 2$, $\mu = 0.3$).

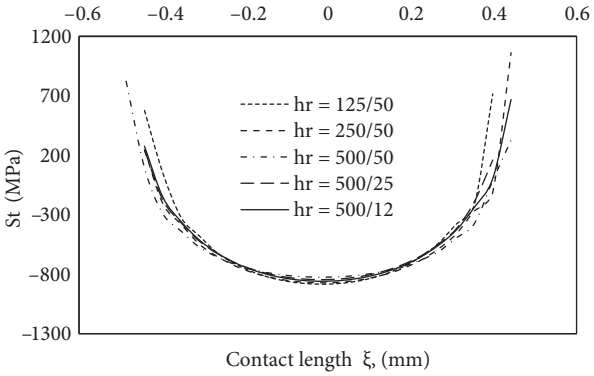

Figure 35. Tangential stress distributions along the contact line of the driven gear for various coating thickness ratios ($R_1 = 225$ mm, $R_2 = 250$ mm, $E_u = E_l = 2$, $\mu = 0.3$).

5. Conclusions

The ball and socket connection is a conforming contact and the material of the coatings and their thicknesses do not affect the displacement and normal stress distributions significantly. The contact friction without horizontal load does not change the symmetry of distributions. However, it reduces the total displacements at the edges of the contact line and it decreases the normal and tangential stresses at the mid-contact region. The horizontal load severely changes the symmetry of distributions in its direction. The tangential stress increases as the ball coating material becomes harder. In addition, it increases when h_r is less than 1.

Ball on a flat plate and roller on a guide are nonconforming contact applications. The coating material and thickness drastically change the displacement and normal and tangential stress distributions along the contact line of coated members. When the coating thickness ratio increases, the displacements increase, but the normal and tangential stresses decrease along the contact line. The normal stresses become nearly the same when the coating materials are swapped. In addition, as the coating material becomes harder, the contact stresses increase, but displacement decreases if the same prescribed displacements are applied.

Gear contact displacements and pressures can be changed by selecting appropriate coating materials and coating thicknesses. The Young's modulus ratio is more effective than coating thickness ratio in contact stresses. However, contact displacements of the tooth are mostly affected by the Young's modulus ratio of the driver tooth. In addition, when the coating thickness ratio is greater than 1, the displacement changes significantly.

The coating and substrate interface is assumed to be perfectly bonded. However, this is not the case in real applications. The quality of the interface region of coating and substrate depends on the coating procedure and requires special attention.

References

Bruno, G., Fanara, C., Guglielmetti, F. and Malard, B., "Characterization and Residual Stress Analysis of Wear Resistant Mo Thermal Spray-Coated Steel Gear Wheels", Surface and Coatings Technology, 200, 4266–4276, 2006.

Diao, D. and Kandori, A., "Finite Element Analysis of the Effect of Interfacial Roughness and Adhesion Strength on the Local Delamination of Hard Coating under Sliding Contact", Tribology International, 39, 849–855, 2006.

Djabella, H. and Arnell, R.D., "Finite Element Analysis of the Contact Stresses in Elastic Coating/Substrate under Normal and Tangential Load", Thin Solid Films, 223, 87–97, 1993.

Guler, M.A. and Erdogan, F., "Contact Mechanics of Two Deformable Elastic Solids with Graded Coatings", Mechanics of Materials, 38, 633–647, 2006.

Gupta, P.K., Walowit, J.A. and Finkin, E.F., "Stress Distribution in Plane Strain Layered Elastic Solids Subjected to Arbitrary Boundary Loading", Journal of Lubrication Technology, 95, 427–432, 1973.

Hong, T. and Saka, N., "Finite Element Analysis of an Elastic Plastic 2-Layer Half-Space-Normal Contact", Wear, 148, 47–68, 1991.

Hsueh, C.H. and Miranda, P., "Combined Empirical–Analytical Method for Determining Contact Radius and Indenter Displacement during Hertzian Indentation on Coating/Substrate Systems", Journal of Materials Research, 19, 2774–2781, 2004.

Johnson, K.L., Contact Mechanics, Cambridge University Press, Cambridge, 1985.

Kanber B., "Analysis of Spur Gears by Coupling Finite and Boundary Element Methods", Mechanics Based Design of Structures and Machines, 34, 307–324, 2006.

Ke L.L. and Wang Y.S., Fretting Contact with Finite Friction of a Functionally Graded Coating with Arbitrarily Varying Elastic Modulus. Part 2: Tangential Loading, J. Strain Analysis, 42, 305–313, 2007.

Komvopoulos, K., "Finite Element Analysis of a Layered Elastic Solid in Normal Contact with a Rigid Surface", Journal of Tribology-Transactions of ASME, 111, 477–485, 1988.

Leroy, J.M. and Villechaise, B., "Stress Determination in Elastic Coatings and Substrate under Both Normal and Tangential Loads, in: Mechanics of Coatings", Tribology Series, Elsevier, Amsterdam, 17, 195–201, 1990.

Lindsay, J.H., Coatings and Coating Processes for Metals, Materials Park, ASM International, OH, 1998.

Liu, C., Bi, Q. and Matthews, A., "Tribological and Electrochemical Performance of PVD Tin Coatings on the Femoral Head of Ti–6Al–4V Artificial Hip Joints", Surface and Coatings Technology, 163–164, 597–604, 2003.

Martins, R.C., Moura, P.S. and Seabra, J.O., "MoS_2/Ti Low-Friction Coating for Gears", Tribology International, 39, 1686–1697, 2006.

Njiwa, R.K., Consiglio, R. and von Stebut, J., "Boundary Element Modelling of a Coating–Substrate Composite under an Elastic, Hertzian Type Pressure Field: Cylinder on Flat Contact Geometry", Surface and Coatings Technology, 102, 138–147, 1998.

O'Sullivan, T.C. and King, R.B., "Sliding Contact Stress Field Due to a Spherical Indenter on a Layered Elastic Half-Space", Journal of Tribology-Transactions of ASME, 110, 235–240, 1988.

Reedy, E.D., "Thin-Coating Contact Mechanics with Adhesion", Journal of Materials Research, 21, 2660–2668, 2006.

Sen, R., Dutta, S., Das, S.K. and Basu, S.K., "Evaluation of a Glass-Ceramic Coating for Machine Tool Slides", Wear, 1, 249–260, 1989.

Shieu, F.S. and Shiao, M.H., "Measurement of the Interfacial Mechanical Properties of a Thin Ceramic Coating on Ductile Substrates", Thin Solid Films, 306, 124–129, 1997.

Sun, Y., Bloyce, A. and Bell, T., "Finite Element Analysis of Plastic Deformation of Various TiN Coating/Substrate Systems under Normal Contact with a Rigid Sphere", Thin Solid Films, 271, 122–131, 1995.

Tian, H. and Saka, N., "Finite Element Analysis of an Elastic Plastic 2-Layer Half-Space-Sliding Contact", Wear, 148, 261–285, 1991.

Wriggers, P., Computational Contact Mechanics, John Wiley & Sons Inc., England, 2002.

Yonekura, D., Chittenden, R.J. and Dearnley, P.A., "Wear Mechanisms of Steel Roller Bearings Protected by Thin, Hard and Low Friction Coatings", Wear, 259, 779–788, 2005.